ACS OMEGA

http://pubs.acs.org/journal/acsodf

Article

Safety Criteria for Solid–Liquid Heterogeneous Systems in Semibatch Reactors

Zheng Ran, Lei Ni, Yong Pan,* Yutong Chen, Jun Wang,* Juncheng Jiang, and Chi-Min Shu

Cite This: *ACS Omega* 2022, 7, 21207–21219

Read Online

ACCESS | Metrics & More | Article Recommendations

ABSTRACT: An exothermic reaction in a semibatch reactor can potentially cause thermal runaway due to evolved energy accumulation or a secondary reaction. This research aims to propose safety criteria for solid–liquid reactions in semibatch reactors. Simulation modeling was carried out to build thermal runaway criteria for solid–liquid reactions in semibatch reactors. A new model for the energy and mass balance of solid–liquid reactions was successfully established. Criteria for the safety boundary diagram and the temperature diagram were ameliorated for solid–liquid reactions. The results showed that the dissolution heat has a great influence on the thermal behavior of the reaction. Experiments to neutralize citric acid and sodium hydroxide were carried out to determine the critical parameters for the neutralization reaction using the temperature diagram criterion. The proposed criteria would be reasonably expected to provide some guidance for chemical process optimization and safety design for engineering.

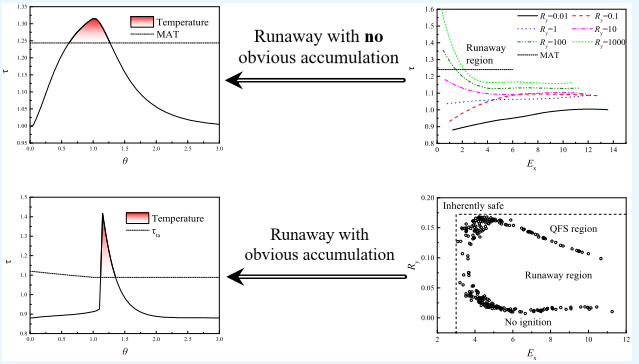

1. INTRODUCTION

Semibatch reactors (SBRs) used in the fine chemical and pharmaceutical industries has been studied extensively. Compared with a batch reactor (BR), a SBR can avoid extreme temperatures by controlling the dosing rate and the cooling temperature.[1] However, thermal runaway accidents are not eliminated completely. Runaway occurs when the operation parameters are set inappropriately.[2,3]

To obtain safe operating conditions, a huge amount of work has been done on safety criteria. Semenov first presented the Semenov criterion in 1928. Considering an exothermal reaction with zero-order kinetics and neglecting the reactant consumption, Semenov provided the Semenov number to obtain the critical temperature.[4] As for SBRs, in 1986, Hugo et al. found that the accumulation of reactants is the main reason for thermal runaway in SBRs and investigated the influence of the breakdown of cooling to the maximum process temperature.[5] Steensma et al. introduced the target temperature (T_{ta}) to verify different thermal behaviors of reactions[6] and proposed a boundary diagram for liquid–liquid homogeneous reactions in SBRs.[7,8] Based on their work, Maestri et al. improved the boundary diagram for liquid–liquid heterogeneous reactions in SBRs[9,10] and proposed an adiabatic temperature diagram by comparing the maximum reaction temperature and the maximum allowable temperature (MAT).[11]

Recently, Ni et al. enhanced the boundary diagram by adding a secondary reaction temperature as the target temperature.[12] Guo et al. defined τ_n as a dimensionless constant temperature to identify the safe operating conditions and predict the maximum temperature of the synthesis reaction (MTSR) at the same time.[13,14] Bai et al. identified four types of reactor thermal behaviors based on the profiles of $MTSR_0$, ϑ_{MTRS}, and the cooling temperature and proposed a new criterion for checking the safer operating conditions of homogeneous reactions in SBRs.[15] After that, Han et al. extended the results of Bai's research to heterogeneous reactions.[16] Zhang et al. proposed a multifeature recognition criterion based on pattern recognition to develop a safety boundary diagram.[17]

In addition, sensitive criteria and divergence criteria have been proposed to forecast thermal runaway.[18,19] Casson et al. compared these works to investigate the hazard of acid-catalyzed esterification and pointed out that these criteria mainly aimed to detect runaway conditions without considering process optimization.[20] Alex et al. summarized the criteria since 1928 and regarded the safety boundary diagram and the

Received: April 6, 2022
Accepted: May 30, 2022
Published: June 8, 2022

temperature diagram as easy and suitable for reactions in SBRs compared with other criteria.[21]

Previous safety boundary diagram- and temperature diagram-related works have generally been proposed for liquid−liquid reactions. Actually, a number of solid−liquid reactions can also have serious consequences due to the massive reaction heat and dissolution heat. The dynamics of solid−liquid reactions in SBRs was first presented by Samoilenko et al. In their study, they investigated the thermal explosion of solid−liquid reactions in a BR[22] and a SBR.[23] However, the mathematical model they proposed did not take into account the influence of dissolution, which can be an exothermic or endothermic process. Besides, the volume of the solid dissolved in the liquid was ignored.

In this paper, first, the dissolution of the solid and the mass and energy balance of solid−liquid reactions was studied in detail. Second, a safety boundary diagram and a temperature diagram were proposed for solid−liquid reactions. Besides, a series of calorimetric experiments were carefully carried out in a SBR to acquire the dissolution heat and the reaction heat. In addition, kinetic and thermodynamic parameters were obtained using Matlab, and the reliability of the theoretical simulation calculation results was demonstrated.

2. RESULTS AND DISCUSSION

2.1. Criteria for the Safety Boundary Diagram and the Temperature Diagram. The thermal safety of solid−liquid reactions in SBRs was assessed both qualitatively and quantitatively using criteria of the safety boundary and the temperature diagram. The necessary steps are listed in Figure 1.

2.1.1. Mathematical Model for Solid−Liquid Reactions in SBRs. In an indirect-cooling SBR, component A is fully dosed from the beginning, while component B is dosed at a constant rate. Here we consider A as the liquid phase and B as the solid phase. A reacts with B to form C and D as products. The reaction heat is removed by a flow of coolant through a jacket.

The mathematical model was formulated on the basis of the following assumptions:

(1) The reaction mass is completely macromixed.
(2) The volume change of the liquid phase is equal to the volume of the dissolved solid.
(3) The heat effects are associated with the chemical reaction and the dissolution of the solid.
(4) The physicochemical properties of all the components are constant during the reaction.
(5) The reaction happens in the liquid phase only.
(6) The heat exchange of the solid reactant completes immediately when dosed into the reactor.
(7) The dosing temperature of the solid is equivalent to the cooling temperature, which remains constant during the entire reaction (the reaction is operated under isoperibolic conditions).

With the assumptions above, reaction conditions can be regarded as ideal. The calculation was simplified with acceptable error, such as the influence of the outside temperature and the change of the reactant's physicochemical properties during the reaction.

In most cases, the dosing rate of solid B (C_B) exceeds the rate of its dissolution into the liquid phase. The concentration of solid B at the interphase surface on the liquid phase side will always be tantamount to its saturation concentration (εC_B).

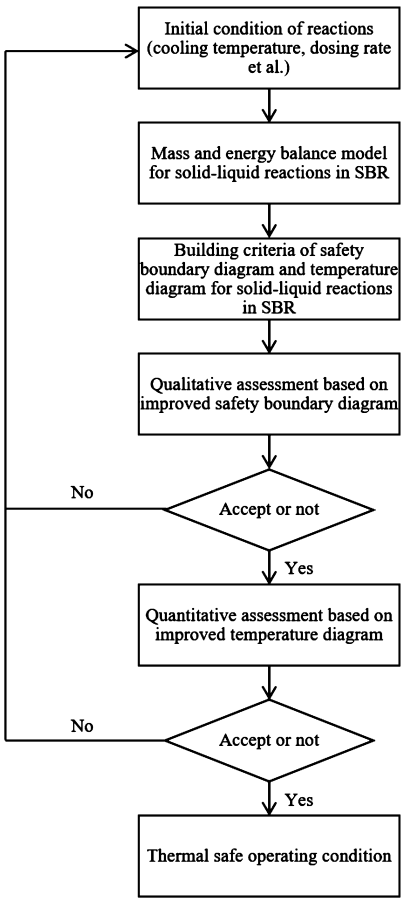

Figure 1. Flowchart of the thermal safety assessment for solid−liquid reactions in SBRs.

The volume of solid B, in turn, that is affected by the dissolution and dosing can be written as shown in eq 1.[24]

$$C_B \frac{dV_B}{dt} = -\delta S(\varepsilon C_B - C_{BA}) + qC_B \quad (1)$$

The interphase surface area of solid B is determined by the volume of solid B and the specific surface area per its unit volume (S_{sp}).

$$S = S_{sp} V_B \quad (2)$$

To determine the specific surface area, it must be calculated as an ensemble of particles (for example, equivalent to spherical particles) with an unknown size distribution. This characteristic of an ensemble of spherical particles is given by eq 3.[24]

$$S_{sp} = \frac{6\mu_2'}{\mu_3'} = \frac{6\int_0^{d_{max}} x^2 f(x)\,dx}{\int_0^{d_{max}} x^3 f(x)\,dx} \quad (3)$$

The value of S_{sp} is calculated by eq 4 based on a Pearson distribution of type I.[24]

$$f(x) = \frac{x^{m_1}(d_{max} - x)^{m_2}}{(d_{max})^{m_1+m_2+1} B(m_1 + 1, m_2 + 1)} \quad (4)$$

where $0 \le x \le d_{max}$, $m_1 + 1 > 0$, $m_2 + 1 > 0$, and $B(m_1 + 1, m_2 + 1)$ is the special β-function. Thus, the second and third

https://doi.org/10.1021/acsomega.2c02139
ACS Omega 2022, 7, 21207−21219

moments of this distribution can be written as eqs 5 and 6, respectively.[24]

$$\mu_2' = d_{max}^2 \frac{(m_1+1)(m_1+2)}{(m_1+m_2+2)(m_1+m_2+3)} \quad (5)$$

$$\mu_3' = d_{max}^3 \frac{(m_1+1)(m_1+2)(m_1+3)}{(m_1+m_2+2)(m_1+m_2+3)(m_1+m_2+4)} \quad (6)$$

Thus, the specific surface area of solid B can be calculated according to eq 7:[24]

$$S_{sp} = \frac{6\mu_2'}{\mu_3'} = 6\frac{(1+\vartheta)}{d_{max}}, \ \vartheta = \frac{(m_2+1)}{(m_1+3)} > 0 \quad (7)$$

The parameter ϑ is a measure of the polydispersity of solid B. When $\vartheta = 0$, the distribution is monodisperse and $S_{sp} = (6/d_{max})V_B$. In this paper, ϑ is assumed to be unity. Thus, the surface area is $S = (12/d_{max})V_B$.

Before the dosing time (t_d), d_{max} is equal to the initial diameter of solid B. After t_d, there is no more solid B dosed into the reactor, and d_{max} changes over time as shown in eq 8.[24]

$$\frac{dd_{max}}{dt} = -2\delta\left(\varepsilon - \frac{C_{BA}}{C_B}\right) \quad (8)$$

For the first stage, solid B is dosed into reactor from t_0 to t_d. The following system of equations was established to describe the dynamic behavior of the reaction system:

Concentration of liquid A dosed at the beginning decreases as reactant B is dosed:

$$\frac{dC_A}{dt} = -\nu_A k_0 \exp\left(-\frac{E_a}{RT}\right) C_A^m C_{BA}^n \quad (9)$$

Concentration of reactant B dissolved in the liquid phase decreases while with reactant A:

$$V_A\frac{dC_{BA}}{dt} = \delta\frac{6V_B(1+\vartheta)}{d_{max}}(\varepsilon C_B - C_{BA}) - \nu_A k_0 \exp\left(-\frac{E_a}{RT}\right) C_A^m C_{BA}^n V_A \quad (10)$$

Volume of solid B dosed constantly decreases as it dissolves in the liquid phase:

$$C_B\frac{dV_B}{dt} = -\delta\frac{6V_B(1+\vartheta)}{d_{max}}(\varepsilon C_B - C_{BA}) + qC_B \quad (11)$$

With above equations, the energy balance equation can be written as follows:

$$c_l\rho_l(V_A+qt)\frac{dT}{dt} = \Delta H_r \nu_A k_0 \exp\left(-\frac{E_a}{RT}\right) C_A^m C_{BA}^n V_A - \alpha(S_0+\Delta s)(T-T_{cool}) + c_s\rho_s q(T_{cool}-T) + \left(C_B\frac{dV_B}{dt} - qC_B\right)\Delta H_{dis} \quad (12)$$

This reveals that the temperature of the reaction system is influenced by four factors: the chemical reaction, the dissolution, the heat removal by the cooling jacket, and the dosing of solid B.

When $t = 0$, the conditions read as

$$C_A = C_{A0}, \ C_{BA} = 0, \ V_B = 0, \ T = T_{cool} \quad (13)$$

The dosing is stopped at t_d when the ratio of moles solid B dosed into the reactor to the initial number of moles liquid A is equal to the stoichiometric ratio. After that, the maximum diameter should be calculated with eq 8. As no more reactant is dosed into the reactor, we need to adjust eqs 9−12) above for the second stage.

$$\frac{dC_A}{dt} = -\nu_A k_0 \exp\left(-\frac{E_a}{RT}\right) C_A^m C_{BA}^n \quad (14)$$

$$V_A\frac{dC_{BA}}{dt} = \delta\frac{6V_B(1+\vartheta)}{d}(\varepsilon C_B - C_{BA}) - \nu_A k_0 \exp\left(-\frac{E_a}{RT}\right) C_A^m C_{BA}^n V_A \quad (15)$$

$$C_B\frac{dV_B}{dt} = -\delta\frac{6V_B(1+\vartheta)}{d}(\varepsilon C_B - C_{BA}) \quad (16)$$

$$c_l\rho_l(V_A+qt)\frac{dT}{dt} = \Delta H_r \nu_A k_0 \exp\left(-\frac{E_a}{RT}\right) C_A^m C_{BA}^n V_A - \alpha(S_0+\Delta s)(T-T_{cool}) + C_B\frac{dV_B}{dt}\Delta H_{dis} \quad (17)$$

$$\frac{dd}{dt} = -2\delta\left(\varepsilon - \frac{C_{BA}}{C_B}\right) \quad (18)$$

At $t = t_d$, the initial values of the reaction system are calculated as the solution of the first stage at $t = t_d$ and the diameter $d = d_{max}$.

According to previous studies, it is necessary to make the above equations dimensionless. Variables were nondimensionalized as shown in eq 19 to make the calculation simple.

$$\eta_A = \frac{C_A}{C_{A0}}, \ \eta_B = \frac{C_{BA}}{C_{A0}}, \ \eta_V = \frac{V_B}{V_A}, \ \eta_d = \frac{d}{d_{max}}, \ \tau = \frac{T}{T_R}, \ \theta = \frac{t}{t_d} \quad (19)$$

For the first stage ($0 < \theta < 1$), the equations for the mass and energy balance are nondimensionalized, as shown in eqs 20−23.

$$\frac{d\eta_A}{d\theta} = -\nu_A D_a \exp\left[\gamma\left(1-\frac{1}{\tau}\right)\right]\eta_A^m \eta_{BA}^n \quad (20)$$

$$\frac{d\eta_B^A}{d\theta} = \frac{d\eta_A}{d\theta} + P_1(1+\vartheta)\frac{\eta_V}{(1+\theta P_2)}\left(\frac{\varepsilon}{P_2} - \eta_B^A\right) \quad (21)$$

$$\frac{d\eta_V}{d\theta} = P_2 - P_1(1+\vartheta)\frac{\eta_V}{(1+\theta P_2)}(\varepsilon - P_2\eta_B^A) \quad (22)$$

$$\frac{d\tau}{d\theta} = -\frac{d\eta_A}{d\theta}\cdot\frac{\Delta\tau_{ad,0}}{1+P_2\theta} - \alpha^* D_a(\tau-\tau_0) - R_H\frac{P_2(\tau-\tau_0)}{1+P_2\theta} - \left(\frac{d\eta_V}{d\theta} - P_2\right)\frac{\Delta\tau_{dis}}{1+P_2\theta} \quad (23)$$

where: $\nu_A D_a = \nu_A t_d K_R C_{A0}$, $\gamma = E_a/(RT_R)$, $P_1 = 6\delta t_d/d_{max}$, $P_2 = C_{A0}/C_B$, $\Delta\tau_{ad,0} = -\Delta H_r n_B/(V_{A0}T_R c_l\rho_l)$, $\Delta\tau dis = -\Delta H_{dis} n_B/(V_{A0}T_R c_l\rho_l)$, $\alpha^* D_a = 2\alpha t D/(r c_l\rho_l))$, and $R_H = c_s\rho_s/(c_l\rho_l))$.

At $\theta = 0$, the initial conditions are

$$\eta_A = 1, \ \eta_B = 0, \ \eta_V = 0, \ \tau_0 = \tau_c \quad (24)$$

https://doi.org/10.1021/acsomega.2c02139
ACS Omega 2022, 7, 21207−21219

For the second stage ($\theta > 1$), the equations are nondimensionalized, as shown in eqs 25−29.

$$\frac{d\eta_A}{d\theta} = -\nu_A D_a \exp\left[\gamma\left(1 - \frac{1}{\tau}\right)\right]\eta_A^m \eta_{BA}^n \tag{25}$$

$$\frac{d\eta_B^A}{d\theta} = \frac{d\eta_A}{d\theta} + \frac{P_1}{\eta_d}(1+\vartheta)\frac{\eta_V}{(1+P_2)}\left(\frac{\varepsilon}{P_2} - \eta_B^A\right) \tag{26}$$

$$\frac{d\eta_V}{d\theta} = -\frac{P_1}{\eta_d}(1+\vartheta)\frac{\eta_V}{(1+P_2)}(\varepsilon - P_2\eta_B^A) \tag{27}$$

$$\frac{d\tau}{d\theta} = -\frac{d\eta_A}{d\theta}\cdot\frac{\Delta\tau_{ad,0}}{1+P_2} - \alpha^* D_a(\tau - \tau_0) - \frac{d\eta_V}{d\theta}\cdot\frac{\Delta\tau_{dis}}{1+P_2} \tag{28}$$

$$\frac{d\eta_d}{d\tau} = \frac{P_1(\eta_B P_2 - \varepsilon)}{3} \tag{29}$$

The initial conditions of eqs 25−29 can be found from the eqs 20−23, respectively, in the former stage. Additionally, $\eta_d = 1$ at $\theta = 1$.

Compared with the mathematical model proposed by Samoilenko,[23] this new model takes into account the change of the volume of the liquid phase caused by the dissolved solid, which can influence the cooling effect of the cooling jacket. Moreover, the new model takes the heat effect of dissolution, which can be an exothermic or endothermic process, into consideration.

2.1.2. Safety Boundary Diagram. Liquid−liquid reactions and solid−liquid reactions share basically same equation for the target temperature, and the trend of each are the same. The temperature decreases as the dosing proceeds and become stable after the dosing is finished, as illustrated by eq 30.

$$\begin{cases} \tau_{ta} = \tau_0 + \dfrac{1.05(\Delta\tau_{ad,0} + \Delta\tau_{dis})}{P_2 R_H + \alpha^* Da(1+P_2\theta)} & \theta \le 1 \\ \tau_{ta} = \tau_0 + \dfrac{1.05(\Delta\tau_{ad,0} + \Delta\tau_{dis})}{P_2 R_H + \alpha^* Da(1+P_2)} & \theta > 1 \end{cases} \tag{30}$$

The reason for this downward trend is the change of the volume and the heat exchange area of the reaction system. In the case of a liquid−liquid reaction, the volume of the reaction system increases as the liquid is dosed into the reactor. The heat exchange area changes as well, thus the quantity of heat can be removed by the cooling jacket. The same as in liquid−liquid reactions, the change is caused by the dosing reactant in solid−liquid reactions. While the solid is dosed into the reactor, it also starts to dissolve, and the volume of the system increases steadily. As the reaction proceeds, the solid is dosed and dissolves into the liquid completely. Eventually, the entire volume of the reaction system is equal to its initial liquid volume plus the volume of the dosed solid, and the target temperature become the same as t_0.

Three characteristic types of thermal behaviors in a SBR were proposed by increasing the cooling temperature compared to T_{ta}, as shown in Figure 2.[25]

By changing the cooling temperature while keeping other conditions unchanged, it is possible to use eq 31 to find a range of cooling temperatures under which the reaction system can cause thermal runaway. Since the safety boundary diagram corresponds to the situation where the τ_{max} is equal to τ_{ta}, it is required to find the condition in compliance with the constraint

$$FF = \tau_{max} - \tau_{ta}|_{\theta(\tau_{max})} \tag{31}$$

As shown in Figure 3, the cooling temperature between the first two roots can lead to the thermal runaway of the system under a certain set of conditions. Thus, by changing the four parameters D_a, $\Delta\tau_{ad,0}$, γ, and P_2 and recording the corresponding roots of the eq 31, we can receive cooling

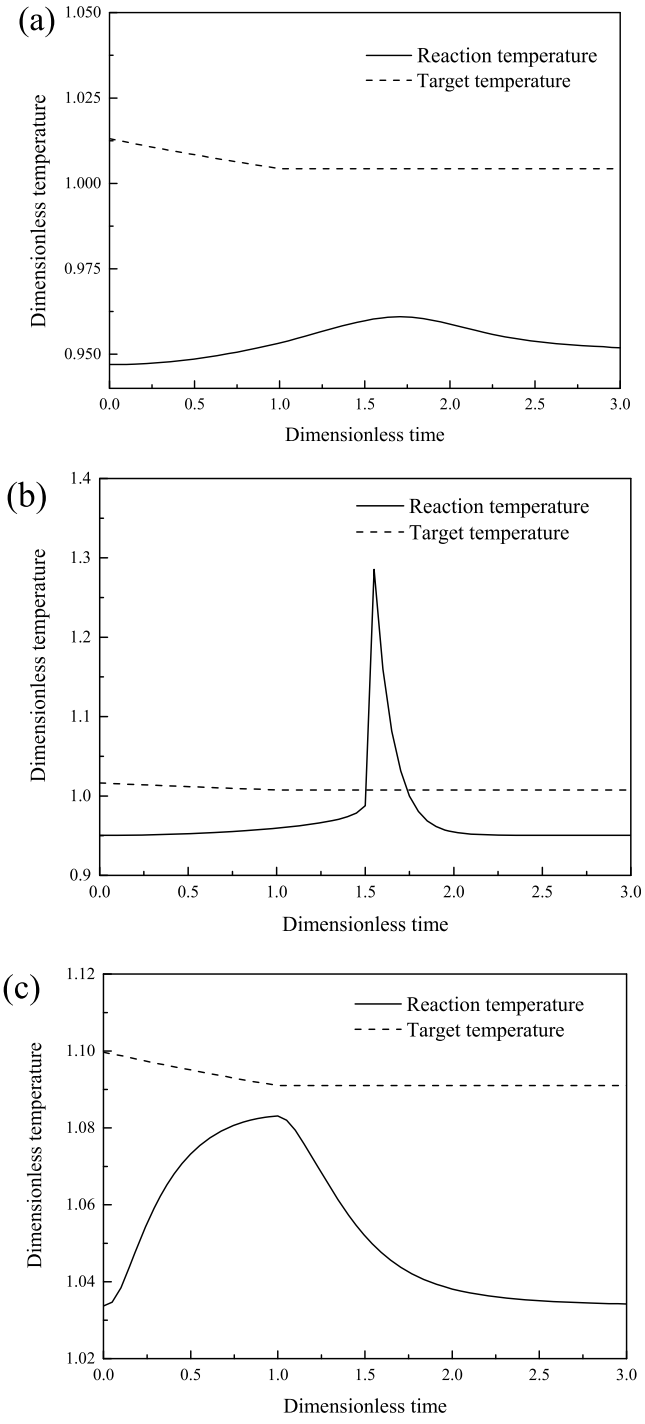

Figure 2. Characteristic diagrams of three thermal behaviors, where $\nu_A D_a = 6.2$, $\gamma = 45.8$, $\Delta\tau_{ad,0} = 0.64$, $\Delta\tau_{dis} = 0$, $\varepsilon = 0.73$, $\vartheta = 1$, $\alpha^* Da = 10$, $R_H = 1$, $P_1 = 1$, $P_2 = 0.155$, $m = 1$, and $n = 1$. (a) No ignition, $T_{cool} = 284$ K. (b) Thermal runaway, $T_{cool} = 285$ K. (c) QFS, $T_{cool} = 310$ K.

https://doi.org/10.1021/acsomega.2c02139
ACS Omega 2022, 7, 21207−21219

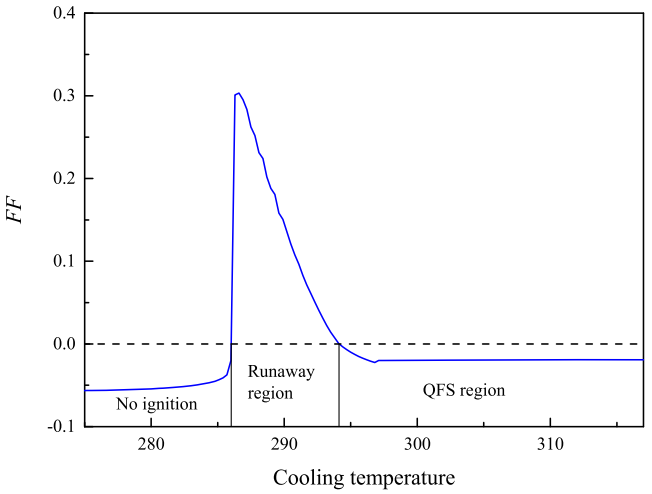

Figure 3. Trend of the FF function for a solid−liquid reaction in a SBR, where $\nu_A D_a = 6.2$, $\gamma = 45.8$, $\Delta\tau_{ad,0} = 0.64$, $\Delta\tau_{dis} = 0$, $\varepsilon = 0.73$, $\vartheta = 1$, $\alpha^* Da = 10$, $R_H = 1$, $P_1 = 1$, $P_2 = 0.155$, $m = 1$, and $n = 1$. The initial reactor temperature and the dosing temperature are equal to the cooling temperature.

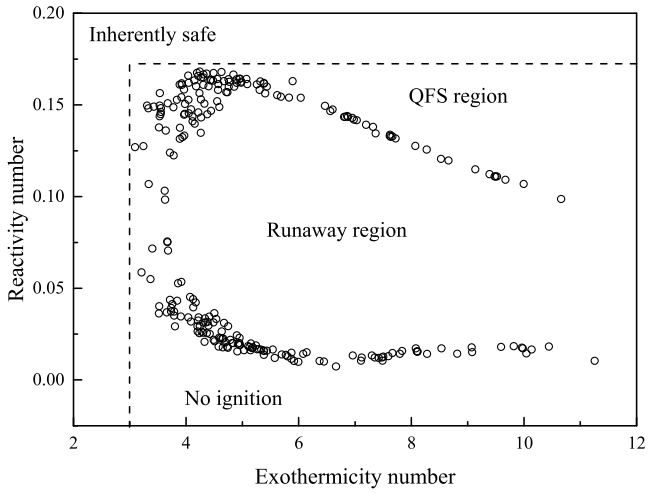

Figure 4. Different thermal behavior regions in a boundary diagram, where $0.025 < \nu_A Da < 18$, $0.1 < \Delta\tau_{ad,0} < 1$, $32 < \gamma < 48$, $0.1 < P_2 < 1$, $\Delta\tau_{dis} = 0$, $\varepsilon = 0.73$, $\vartheta = 1$, $\alpha^* Da = 10$, $R_H = 1$, $P_1 = 1$, $m = 1$, and $n = 1$.

temperature intervals that can cause thermal runaway for different conditions.

Based on the research of Steensma and Westerterp,[6] the reactivity factor (F_R), the exothermicity factor (F_E), the dissolution factor (F_D), the cooling factor (F_{cool}), the exothermicity number (E_x), and the reactivity number (R_y) of solid−liquid reaction are as follows:

$$F_R = \nu_A Da \exp\left[\gamma\left(1 - \frac{1}{\tau_0}\right)\right] \tag{32}$$

$$F_E = \Delta\tau_{ad,0}\frac{\gamma}{\tau^2} \tag{33}$$

$$F_D = \Delta\tau_{dis} \tag{34}$$

$$F_{cool} = P_2 R_H + \alpha^* D_a(1 + P_2\theta) \tag{35}$$

$$E_x = \left.\frac{F_E + F_D}{F_{cool}}\right|_{\theta=0} = \frac{\Delta\tau_{ad,0}\frac{\gamma}{\tau_0^2} + \Delta\tau_{dis}}{P_2 R_H + \alpha^* D_a(1 + P_2\theta)} \tag{36}$$

$$R_y = \left.\frac{F_R}{F_{cool}}\right|_{\theta=0} = \frac{\nu_A D_a \exp\left[\gamma\left(1 - \frac{1}{\tau_0}\right)\right]}{P_2 R_H + \alpha^* D_a(1 + P_2\theta)} \tag{37}$$

The boundary diagram can be established by putting the roots from eq 31 into eqs 36 and 37. Figure 4 is an example boundary diagram. Three thermal behaviors are shown, and an inherently safe region is divided by the dashed line.

2.1.3. Temperature Diagram. In addition to T_{ta}, maximum allowed temperature (MAT) is also used to define the thermal behavior. A reaction with a maximum temperature over the MAT is considered to have thermal runaway. Using the boundary diagram, we can judge whether the reaction is out of control because of its accumulation, but sometimes the reaction temperature can reach MAT without an obvious accumulation. To quantitatively describe the maximum reaction temperature under different conditions, a temperature diagram was proposed by Maestri and Rota.[11]

Figure 5a displays temperature diagrams developed under certain conditions, where the lines are the fitting results. A line of the MAT, which is often chosen as the boiling point of

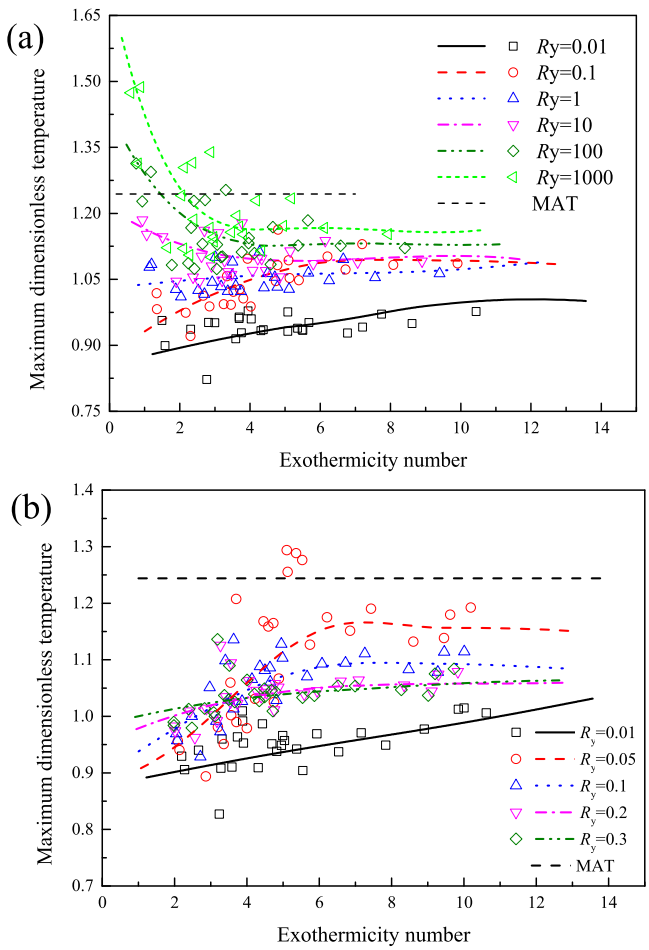

Figure 5. Temperature diagrams for solid−liquid reactions in a SBR, where $0.025 < \nu_A Da < 18$, $0.1 < \Delta\tau_{ad,0} < 1$, $32 < \gamma < 48$, $0.1 < P_2 < 1$, $\Delta\tau_{dis} = 0$, $\varepsilon = 0.73$, $\vartheta = 1$, $\alpha^* Da = 10$, $R_H = 1$, $P_1 = 1$, $m = 1$, and $n = 1$. (a) $R_y = 0.01$, 0.1, 1, 10, 100, and 1000. (b) $R_y = 0.01$, 0.05, 0.1, 0.2, and 0.3.

https://doi.org/10.1021/acsomega.2c02139
ACS Omega 2022, 7, 21207−21219

water, was drawn. As shown in Figure 5a, the reaction can reach the MAT at a low E_x and a high R_y. This is mainly caused by a high cooling temperature. In addition, the curve of R_y = 0.1 exceeds the curve of R_y = 1 in a certain interval of E_x because of its accumulation. For R_y = 0.01−0.3, there is the possibility that the maximum temperature can exceed the MAT, as shown in Figure 5b.

2.2. Influence of the Dissolution Heat. Calculating the heat of dissolution of various substances can be extremely different. For an electrolyte, the dissolution involves ionization and hydration processes, which are endothermic and exothermic, respectively. Thus, according to the intensity of ionization and hydration, the dissolution heat can be negative, such as $Al_2(SO_4)_3$ with a dissolution heat of −527 kJ mol^{-1}, or positive, such as $Na_2HPO_4{\cdot}12H_2O$ with a dissolution heat of 97 kJ mol^{-1}. As shown in Figure 6, the dissolution heat can be

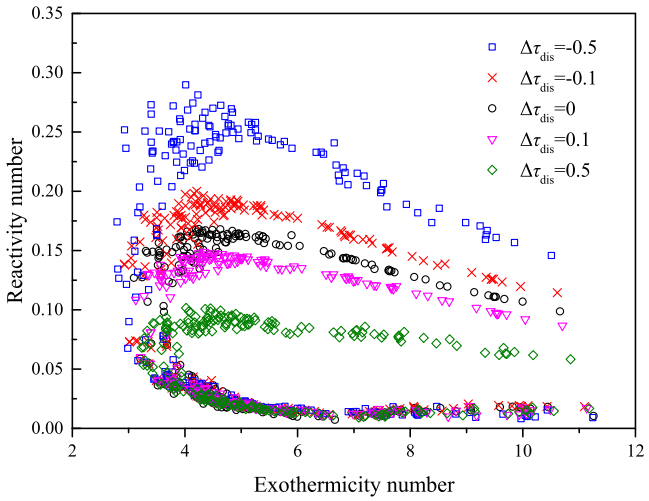

Figure 6. Generalized boundary diagram with different $\Delta\tau_{dis}$ values, where $0.025 < \nu_A Da < 18$, $0.1 < \Delta\tau_{ad,0} < 1$, $32 < \gamma < 48$, $0.1 < P_2 < 1$, ε = 0.73, ϑ = 1, $\alpha^* Da$ = 10, R_H = 1, P_1 = 2, m = 1, and n = 1.

so intense, even more than the reaction heat sometimes, that is has a great influence on the boundary diagram. The minimum R_y values of reactions with different dissolution heats had very little difference, but the maximum value of R_y increases as $\Delta\tau_{dis}$ decreases. Futhermore, the minimum E_x also became lower slightly as $\Delta\tau_{dis}$ decreased. This meant that the runaway region became larger when the reaction had an endothermic dissolution, and the reaction was more likely to accumulate and cause thermal runaway. Figure 7 shows profiles of temperature diagrams with different $\Delta\tau_{dis}$ values, and Figure 8 compares three R_y lines under three values of $\Delta\tau_{dis}$. From the figures, we can know that the influence of $\Delta\tau_{dis}$ on the minimum R_y in the boundary diagram is that the minimum R_y decreases as $\Delta\tau_{dis}$ increases.

Combining the boundary diagram and the temperature diagram, we can draw the conclusion that endothermic dissolution is advantageous for thermal runaway caused by accumulation but is also able to lower the temperature for reactions that are not likely to accumulate. Conversely, exothermic dissolution is not only helpful for preventing the reaction from experiencing thermal runaway caused by accumulation but is also likely to heat the reaction to the MAT without accumulation.

A comparison of the elaborated safety diagram and temperature diagram to other criteria is shown in Table 1. The criteria of divergence and Morbidelli−Varma were compared with the safety boundary diagram by Westerterp et al.[13] The result showed that the divergence criterion is too conservative, indicating a higher T_{cool} as a critical temperature. The results of the Morbidelli−Varma criterion and the safety diagram were well-matched. However, it takes a tremendous amount of work to execute the numerical simulations required for the Morbidelli−Varma criterion. Thus, the safety boundary diagram is an efficient and robust method of obtaining safe operating conditions.

2.3. Experimental Validation. Figure 9 presents the temperature and the heat flow profile for the dissolution of NaOH and citric acid (CA). The ΔH_{dis} values of NaOH and CA calculated by integrating the heat flow were −40.8 and 21.1 kJ mol^{-1}, respectively. The temperature trendindicated that exothermic or endothermic dissolution can be serious and should not be ignored. The mass transfer coefficients (δ) of NaOH and CA were calculated to be 0.00687 and 0.00532 cm s^{-1}, respectively, using eq 11.

The calorimetry experiment was conducted to analyze thermal behaviors of the neutralization of CA and NaOH under various cooling temperatures and dosing rates. As shown in Figure 10, CA was dosed as the substrate, and the temperature increased as NaOH was dosed into the reactor, reaching the maximum temperature at t_d. The cooling temperature was set at 282.15, 287.15, 292.15, 297.15, or 302.15 K, but the maximum temperature had no notable difference and the temperature trends were also the same. This meant that the neutralization of CA and NaOH was not sensitive to the cooling temperature and that the reaction rate was too quick for NaOH to accumulate. Accordingly, its thermal behavior did not change much under different cooling temperatures. Therefore, changing the cooling temperature had little effect on the reaction process for the neutralization of CA and NaOH.

Figure 11 shows the thermal behavior of the neutralization of CA and NaOH at different dosing rates. The same as Figure 10, the temperature increased as NaOH was dosed into the reactor and reached the maximum temperature at t_d. However, the maximum temperature decreased when the dosing rate was set lower. Thus, it was possible to control the reaction process by lowering the dosing rate to avoid thermal runaway.

When the substrate changed from the 38.4% w/v CA solution to the 24% w/v NaOH solution with the same dosing time and cooling temperature, the maximum temperature was found to be much lower, as shown in Figure 12. The huge difference between the maximum temperatures of the experiments was caused by the dissolution of the solid. The ΔH_{dis} of NaOH measured previously is −40.8 kJ mol^{-1}, making it an exothermic process, while the ΔH_{dis} of CA measured previously is 21.1 kJ mol^{-1}, making it an endothermic process. As a result, the maximum temperature with the NaOH solution as the substrate is about 18.5 K lower than that with the CA solution as the substrate due to the difference between the ΔH_{dis} values of CA and NaOH.

Using eqs 20−29 and the experimental data, $\Delta H_{r,cal}$ was calculated to be −55.7 kJ mol^{-1} and$\Delta H_{r,exp}$ was found to be −96.5 kJ mol^{-1}, respectively. The kinetic parameters for the neutralization of CA and NaOH, as shown in in Table 2, were calculated using Matlab and Origin. The simulation results are shown in Figure 13, where the solid lines represent

https://doi.org/10.1021/acsomega.2c02139
ACS Omega 2022, 7, 21207−21219

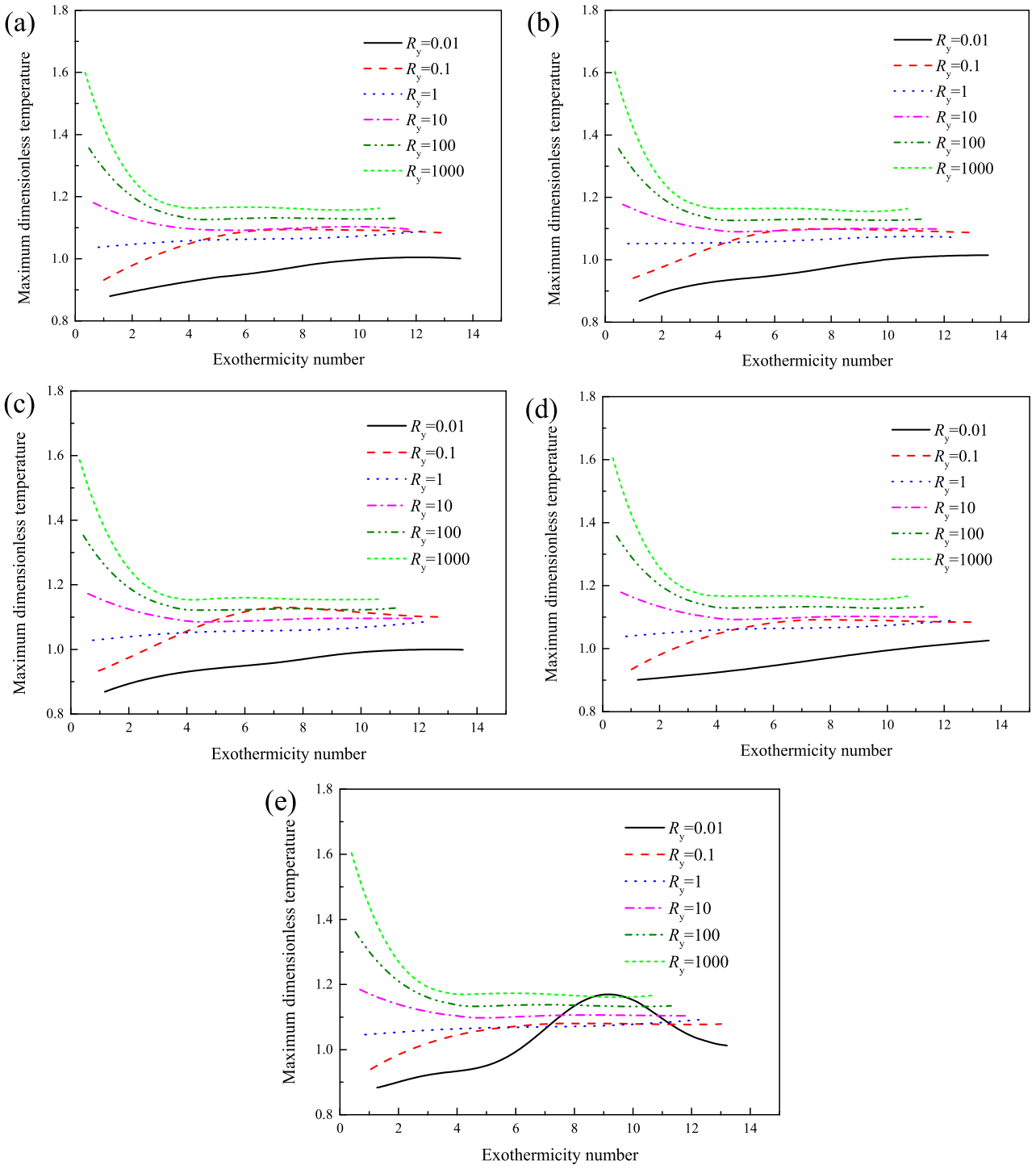

Figure 7. Temperature diagrams with different $\Delta\tau_{dis}$ values, where $0.025 < \nu_A Da < 18$, $0.1 < \Delta\tau_{ad,0} < 1{,}32 < \gamma < 48$, $0.1 < P_2 < 1$, $\varepsilon = 0.73$, $\vartheta = 1$, $\alpha^* Da = 10$, $R_H = 1$, $P_1 = 2$, $m = 1$, and $n = 1$. (a) $\Delta\tau_{dis} = 0$, (b) $\Delta\tau_{dis} = -0.1$, (c) $\Delta\tau_{dis} = -0.5$, (d) $\Delta\tau_{dis} = 0.1$, and (e) $\Delta\tau_{dis} = 0.5$.

experimental temperature trends and the dashed lines represent simulation temperature trends. It can be seen that the simulation temperature trends were close to the experimental temperature trends, indicating that the model proposed earlier has a sound goodness of fitting.

Some reaction parameters, such as the cooling coefficient were given by the calorimeter (RC1^e) directly, while the others were calculated earlier in this article using the experimental results. E_x and R_y can be calculated using eqs 36 and 37, respectively, after nondimensionalizing the reaction parameters. The calculated experimental results are listed in Table 3.

As there was no obvious accumulation during the reaction, a temperature diagram is more appropriate for the neutralization of CA and NaOH. The reaction parameters used to judge the thermal behaviors and the results can be seen in Figure 14. Using the temperature diagrams, the critical cooling temperature with a dosing rate of 30 g min^{-1} was inferred to be 303.276 K, and the critical dosing rate with a cooling temperature of 292.15 K was inferred to be 37.585 g min^{-1}.

https://doi.org/10.1021/acsomega.2c02139
ACS Omega 2022, 7, 21207−21219

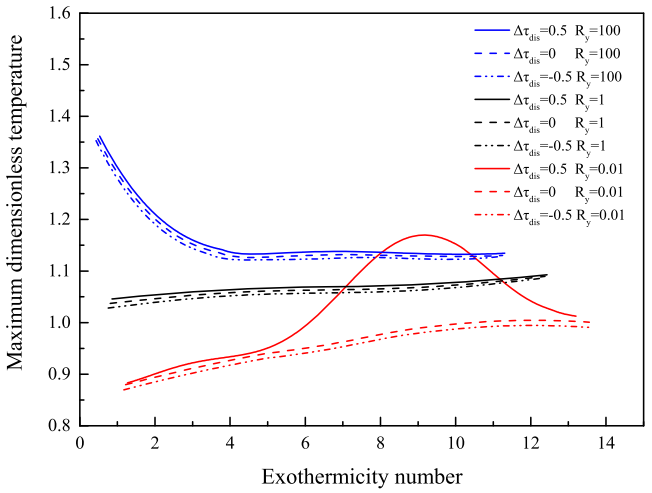

Figure 8. Generalized temperature diagram with different $\Delta\tau_{dis}$ values, where $0.025 < \nu_A Da < 18$, $0.1 < \Delta\tau_{ad,0} < 1{,}32 < \gamma < 48$, $0.1 < P_2 < 1$, $\varepsilon = 0.73$, $\vartheta = 1$, $\alpha^* Da = 10$, $R_H = 1$, $P_1 = 2$, $m = 1$, and $n = 1$.

3. CONLUSIONS

In this study, safety criteria were proposed for solid−liquid heterogeneous systems in semibatch reactors. An energy and mass balance dimensionless mathematical model for solid−liquid reactions in SBRs was successfully established and used to ameliorate the boundary diagram and temperature diagram criteria. In addition to the reactive factor (F_R) and the exothermicity factor (F_E), the dissolution factor (F_D) was added to contain information on the dissolution heat. The critical thermal runaway condition is T_{ta} for the boundary diagram and the MAT for temperature diagram. Based on the result of the boundary diagram, it was found that the runaway region was smaller when the dissolution was exothermic, indicating that exothermic dissolution was advantageous to prevent runaway caused by the accumulated reactant. Based on the result of the temperature diagram, it was found that reactions were more likely to reach the MAT with endothermic dissolution when there was no obvious accumulation in the reactor. The two criteria are fairly related from the points of view of both calculation and application; to obtain the safe operating conditions in a SBR, the temperature diagram should be applied first to check the relationship between the reaction temperature and the MAT value. Then, the boundary diagram should be used as a quantitative judgment for runaway caused by the accumulated reactant.

Calorimetry experiments for the neutralization of CA and NaOH were carried out to obtain the thermodynamic and kinetic parameters. By comparing the experimental results and the simulation results, the proposed criteria were shown to be in a good agreement with the practical situation. Using the temperature diagram criterion, the critical conditions were determined to be a cooling temperature of 303.28 K and a dosing rate of 37.59 g min^{-1}=. This work would be reasonably expected to provide some guidance for process safety design and thermal runaway prevention in semibatch reactors.

4. MATERIALS AND METHODS

4.1. Establishment of Criteria. Before building the criteria, it is necessary to predict the thermal behavior of reactions with a mathematical model. In view of solid−liquid reactions, the mathematical model includes the dissolution of the solid and the mass and energy balance of the reaction. The equations in the model can be solved by ode23 (Bogacki−Shampine) in Matlab using Runge−Kutta methods. This algorithm is better than ode45 in terms of allowable error and the calculation of rigid problems.

Based on the studies by Maestri and Rota,[26,27] T_{ta} was introduced as the target temperature. Based on a comparison of the maximum reaction temperature and T_{ta}, the following three characteristic types are proposed for thermal behavior in a SBR:

(1) No ignition: with a low cooling temperature, the reaction temperature is always lower than the corresponding target temperature. The reaction is too slow to cause thermal runaway in this condition, although the accumulation of the reactant can reach a high value.

(2) Runaway region: as the cooling temperature increases further, the rate of the reaction is not low enough to avoid thermal runaway but is also not high enough to keep the accumulation at an acceptable value. Under this situation, thermal runaway of the reaction system may occur.

(3) QFS region: The reaction rate is high enough to avoid thermal runaway by keeping the accumulation sufficiently low as an ideal condition. This situation is referred to as a quick onset, fair conversion, smooth temperature profile (QFS) situation because the reaction temperature swiftly approaches the target temperature but will not exceed it.

By changing the cooling temperature while keeping other conditions unchanged, it is possible to find a range of cooling temperatures under which the reaction system can cause thermal runaway. When the maximum reaction temperature is equal to T_{ta}, the corresponding cooling temperature is regarded as the critical temperature. To obtain the critical temperature under different conditions, the parameters $\nu_A D_a$, $\Delta\tau_{ad,0}$, γ, and P_2 were changed randomly in a certain interval. The exothermicity number E_x and the reactivity number R_y were calculated, and the operating parameters and the boundary

Table 1. Comparison of Several Criteria

criterion	advantages	disadvantage
divergence criterion	can be applied for several types of reactors	too conservative
Morbidelli−Varma criterion	able to reflect the influence of different parameters on the reaction system	complicated calculation
Samoilenko's work	able to determine critical conditions of thermal ignition for solid−liquid reactions in SBRs and BRs	ignores the influence of the dissolution process on the temperature and volume of the reaction system
safety boundary and temperature diagram criteria	convenient to use and the results are intuitive	cannot be applied for solid−liquid reactions
criteria proposed in this study	able to obtain safe operating conditions of solid−liquid reactions in SBRs qualitatively and quantitatively	cannot be applied for reactions in other reactors

https://doi.org/10.1021/acsomega.2c02139
ACS Omega 2022, 7, 21207−21219

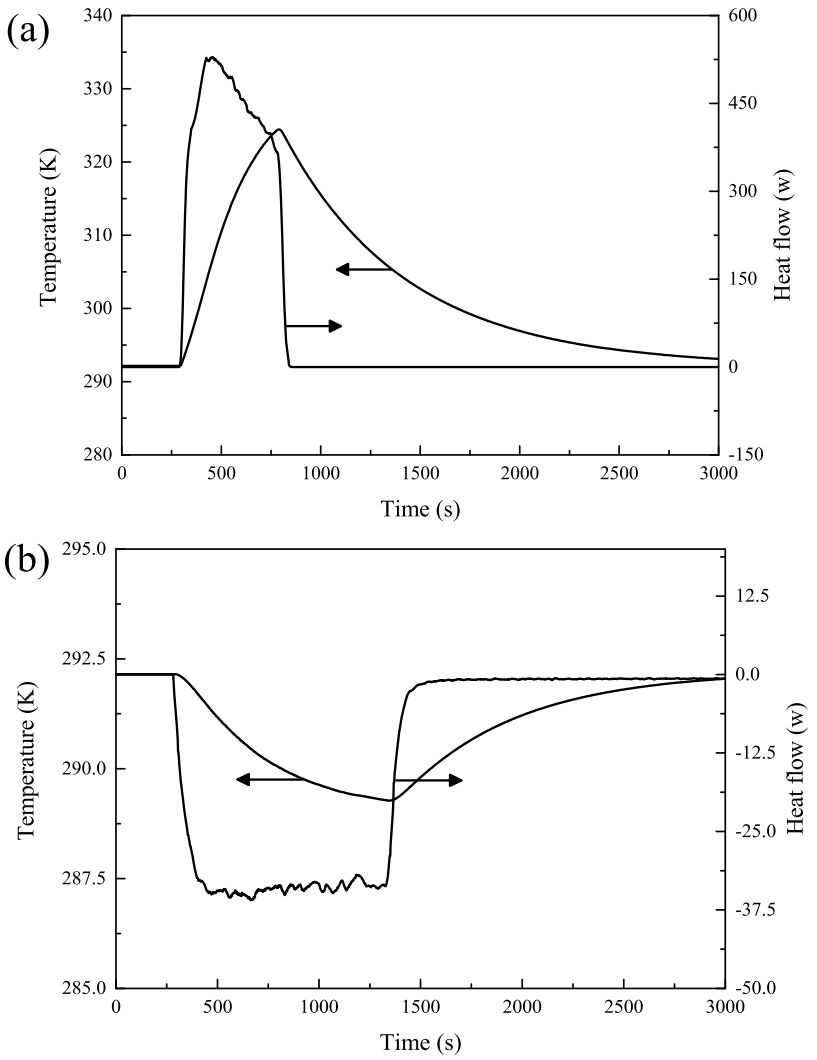

Figure 9. Temperature and heat flow profiles for the dissolution of (a) NaOH and (b) CA in water.

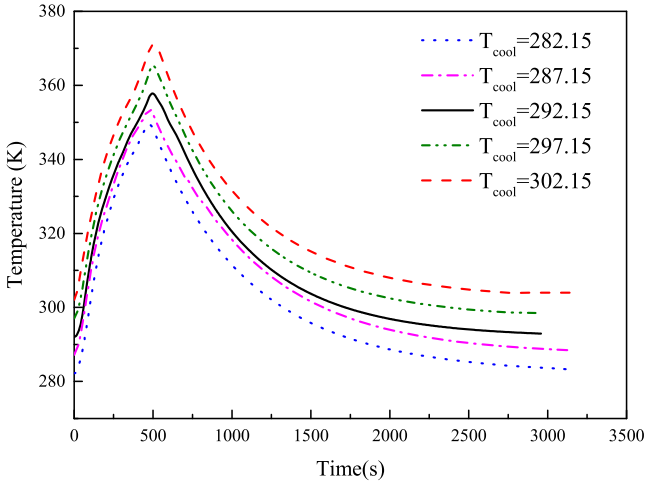

Figure 10. Temperature vs time profiles with different cooling temperatures.

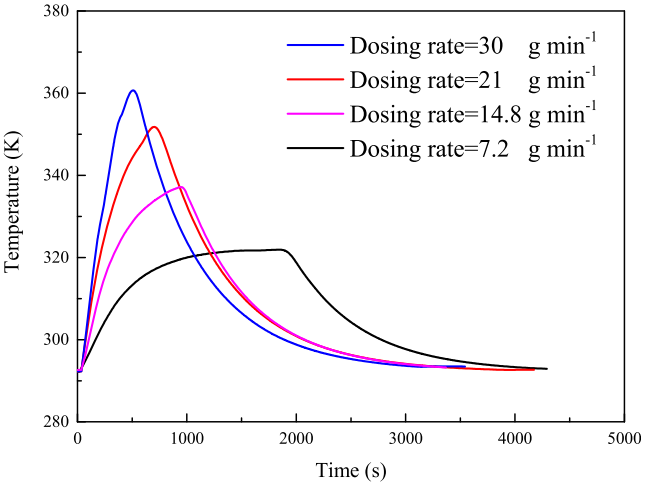

Figure 11. Temperature versus time profiles with different dosing rates.

diagram can be built using E_x and R_y as coordinates, respectively.

To build a temperature diagram, the same dimensionless parameters are used (i.e., the exothermicity number E_x and the reactivity number R_y). First, a set of parameters, namely $\nu_A D_a$, $\Delta\tau_{ad,0}$, $\Delta\tau_{dis}$, γ, P_1, P_2, ϑ, ϵ, $\alpha^* D_a$, R_H, m, and n, is assigned in compliance with an acceptable range. A certain value is chosen for R_y, and the cooling temperature and E_x can be calculated

https://doi.org/10.1021/acsomega.2c02139
ACS Omega 2022, 7, 21207−21219

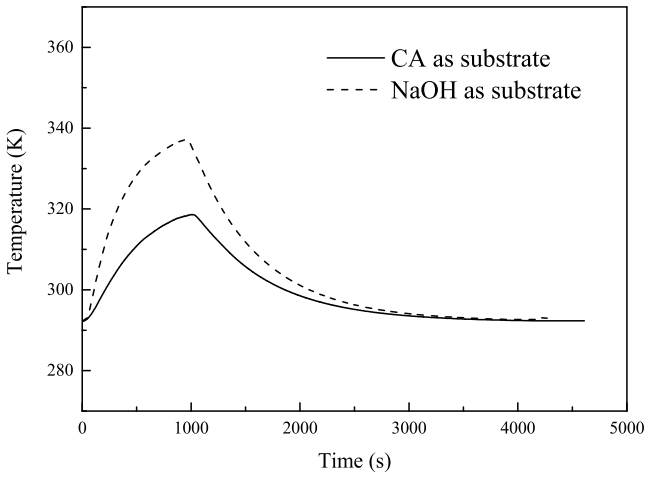

Figure 12. Temperature versus time profiles with different substrates.

Table 2. Kinetic Parameters Calculated by Matlab for the Neutralization of CA and NaOH

kinetic parameter	value
apparent activation energy (E_a)	46.9 kJ mol^{-1}
pre-exponential factor (A)	2.79 × 10^{10} (cm^3 mol^{-1})^3 s^{-1}
reaction order (NaOH)	3
reaction order (CA)	1

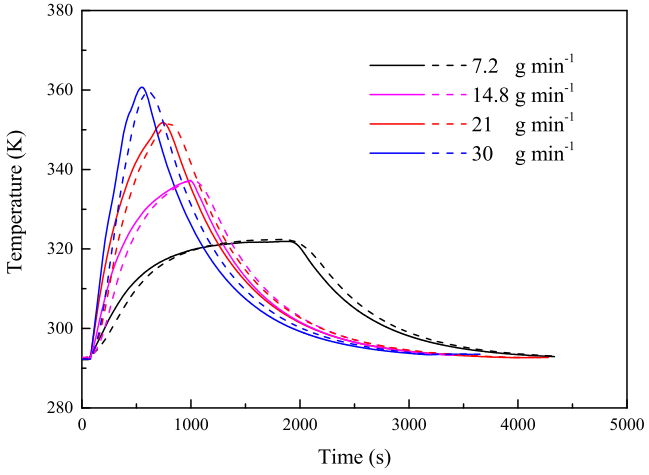

Figure 13. Comparison of fitting results and experimental data for different dosing rates.

Table 3. Dimensionless Experimental Results of R1-R8

reaction	dimensionless maximum temperature	E_x	R_y
R1	1.159	1.768	16.728
R2	1.172	1.715	18.626
R3	1.192	1.664	20.664
R4	1.217	1.616	22.844
R5	1.236	1.569	25.171
R6	1.073	1.214	21.097
R7	1.124	0.863	21.435
R8	1.173	0.439	21.842

using eqs 36 and 37, respectively. The parameters $\nu_A D_a$, $\Delta\tau_{ad,0}$, γ, and P_2 were changed randomly in a certain interval while the remaining six parameters (i.e., $\Delta\tau_{dis}$, P_1,ϑ, ε, $\alpha^* D_a$, and R_H) were kept constant, and the above procedure was repeated to

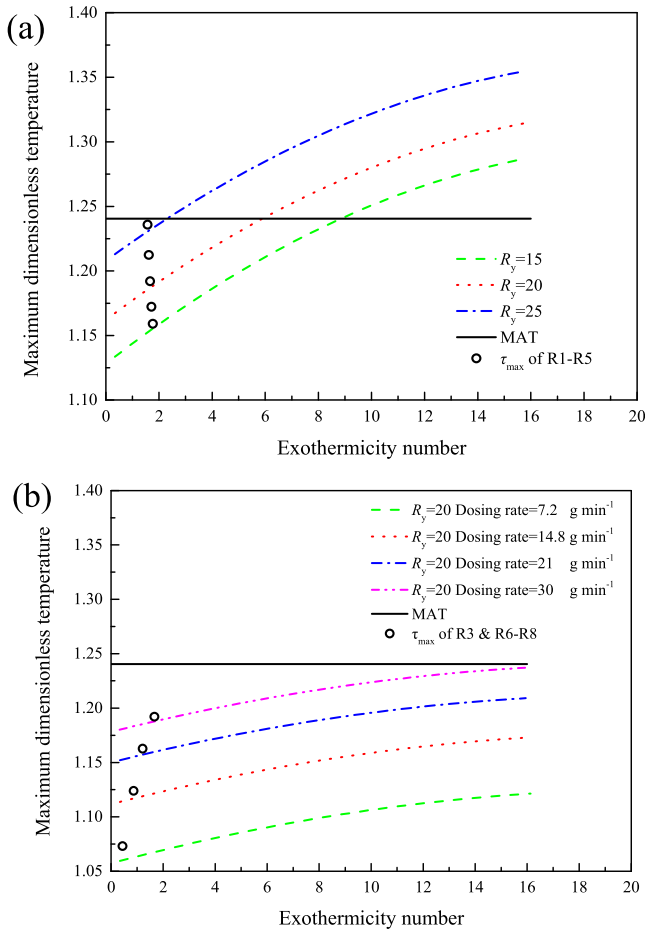

Figure 14. Positions of experimental results in the temperature diagram. (a) Results of R1−R5 and (b) results of R3 and R6−R8.

find different cooling temperatures and values E_x for a certain value of R_y. The temperature diagram can be built with E_x and the maximum reaction temperature as coordinates.

4.2. Calorimetry Experiment. *4.2.1. Reaction and Materials.* The acid−base neutralization reaction of CA and NaOH is widely used for sodium citrate production and is also a typical exothermic solid−liquid reaction.[28] In this study, the neutralization reaction of CA and NaOH was chosen to prove the reliability of the proposed models. NaOH was purchased from Sinopharm Chemical Reagent Co. (A.R.), and CA was purchased from Macklin Reagent Co. (A.R.). The particle sizes were measured with micrometer to be 1.055 (NaOH) and 1.436 mm (CA).

4.2.2. Apparatus and Calorimetric Tests. The integral dissolution heat of NaOH and CA was measured using a reaction calorimeter (RC1^e, Mettler Toledo Ltd., Switzerland) with a Lambda Doser powder dosing instrument (Lambda Laboratory Instruments Ltd., Czech Republic). The experiment began with the addition of 1 L of water into the reactor. The stirring rate was set at 200 rpm, and the heat transfer coefficient and specific heat were determined by a thermal calibration procedure. Then, 6 mol NaOH was dosed at a rate of 30 g min^{-1} with a cooling temperature of 292.15 K. The integral dissolution heat of CA was also obtained with the same procedure. Roughly, 2 mol CA was dosed at a rate of 22.8 g min^{-1} with a cooling temperature of 292.15 K. The heat transfer coefficient and the specific heat were determined again

https://doi.org/10.1021/acsomega.2c02139
ACS Omega 2022, 7, 21207−21219

when the dosing was finished. The experimental data were analyzed using eq 38.

$$\Delta H_{dis} = \frac{\int_{t_0}^{t_e} q_{hf}\, dt}{n_s} \quad (38)$$

The acid−base neutralization of CA and NaOH was performed in RC1^e with the Lambda doser powder dosing instrument. The experimental conditions are summarized in Table 4. Approximately 1 L of the 38.4% w/v CA solution (2 mol) was prepared and dosed into the reactor first. The heat transfer coefficient and the specific heat were determined using a thermal calibration procedure with the stirring rate of 200 rpm. The reactor was cooled to the set temperature. After 10 min of stabilization, 6 mol NaOH was dosed under the set rate. The heat transfer coefficient and the specific heat were determined again when the reaction was finished. To observe the influence of the dosing reactants, we changed the substrate from 1 L of the 38.4% w/v CA solution to 1 L of the 24% w/v NaOH solution (6 mol), and the dosing rate was set at 23.6 g min^{-1} at 292.15 K. The stoichiometric scheme for the acid−base neutralization of CA and NaOH is given by eq 39.

Table 4. Experimental Conditions for the Acid−Base Neutralization of CA and NaOH in RC1^e

reaction	cooling temperature (K)	substrate	dosing reactant	dosing rate (g min^{-1})	dosing time (min)
R1	282.15	CA	NaOH	30	8
R2	287.15	CA	NaOH	30	8
R3	292.15	CA	NaOH	30	8
R4	297.15	CA	NaOH	30	8
R5	302.15	CA	NaOH	30	8
R6	292.15	CA	NaOH	21	11.4
R7	292.15	CA	NaOH	14.8	16.3
R8	292.15	CA	NaOH	7.2	33.3
R9	292.15	NaOH	CA	23.6	16.3

$$3NaOH + C_6H_8O_7 \rightarrow C_6H_5Na_3O_7 + 3H_2O \quad (39)$$

The reaction enthalpy can be calculated by integrating the heat flow with eqs 40 and 41.

$$\Delta H_{r,exp} = \frac{\int_{t_0}^{t_e} q_{hf}\, dt}{n_s} \quad (40)$$

$$\Delta H_{r,exp} = \Delta H_{r,cal} + \Delta H_{dis} \quad (41)$$

AUTHOR INFORMATION

Corresponding Authors

Yong Pan − *College of Safety Science and Engineering, Nanjing Tech University, Nanjing, Jiangsu 211816, China;* orcid.org/0000-0002-6544-1443; Phone: +86-025-83239976; Email: yongpan@njtech.edu.cn

Jun Wang − *College of Safety Science and Engineering, Nanjing Tech University, Nanjing, Jiangsu 211816, China;* Phone: +86-025-83239951; Email: jwang@njtech.edu.cn

Authors

Zheng Ran − *College of Safety Science and Engineering, Nanjing Tech University, Nanjing, Jiangsu 211816, China*

Lei Ni − *College of Safety Science and Engineering, Nanjing Tech University, Nanjing, Jiangsu 211816, China*

Yutong Chen − *College of Safety Science and Engineering, Nanjing Tech University, Nanjing, Jiangsu 211816, China*

Juncheng Jiang − *College of Safety Science and Engineering, Nanjing Tech University, Nanjing, Jiangsu 211816, China; School of Environment and Safety Engineering, Changzhou University, Changzhou, Jiangsu 213164, China;* orcid.org/0000-0001-7018-2709

Chi-Min Shu − *Department of Safety, Health, and Environmental Engineering, National Yunlin University of Science and Technology, Yunlin 64002 Taiwan, ROC;* orcid.org/0000-0001-9455-6162

Complete contact information is available at: https://pubs.acs.org/10.1021/acsomega.2c02139

Notes

The authors declare no competing financial interest.

ACKNOWLEDGMENTS

This research was supported by the Natural Science Foundation for Distinguished Young Scholars of Jiangsu Province (no. BK20190036) and the National Natural Science Foundation of China (no. 51974165). Z.R. is grateful for the support of the Postgraduate Research and Practice Innovation Program of Jiangsu Province (no. SJCX21_0437).

NOMENCLATURE

Latin Symbols

A pre-exponential factor (cm^3 mol^{-3} s^{-1})
c_l specific heat capacity of the liquid phase (J g^{-1} K^{-1})
c_s specific heat capacity of the solid phase (J g^{-1} K^{-1})
C_A concentration of reactant A (mol·m^{-3})
C_{A0} initial concentration of reactant A (mol·m^{-3})
C_B concentration of reactant B (mol m^{-3})
C_{BA} concentration of reactant B in the liquid phase (mol m^{-3})
D_a Damköhler number (J mol^{-1})
d diameter (m)
d_{max} maximum diameter (m)
E_a activation energy (J mol^{-1})
E_x exothermicity number
FF function to identify the critical temperatures
F_R reactivity factor
F_E exothermicity factor
F_D dissolution factor
F_{cool} cooling factor
ΔH_r reaction enthalpy (J mol^{-1})
$\Delta H_{r,exp}$ experimental reaction enthalpy (J mol^{-1})
$\Delta H_{r,cal}$ calculated reaction enthalpy (J mol^{-1})
ΔH_{dis} dissolution enthalpy (J mol^{-1})
k_0 kinetic rate constant (mol L^{-1} s^{-1})
m reaction order of reactant A
n reaction order of reactant B
n_A number of molar equivalents of reactant A (mol)
n_B number of molar equivalents of reactant B (mol)
n_s number of molar equivalents of the solid reactant (mol)
P_1 dimensionless parameter of the dissolution rate
P_2 concentration ratio of reactant A to reactant B
q dosing rate (g min^{-1})
q_{hf} exothermic rate (w)
R ideal gas constant (8.314 J mol^{-1} K^{-1})

https://doi.org/10.1021/acsomega.2c02139
ACS Omega 2022, 7, 21207−21219

R_H dimensionless heat capacity ratio
R_y reactivity number
S heat exchange surface area (m^2)
S_{sp} heat exchange specific surface area (m^2 m^{-3})
S_0 initial heat exchange surface area (m^2)
t time (s)
t_0 initial time (s)
t_d dosing time (s)
t_e ending time (s)
T temperature (K)
T_{cool} cooling temperature (K)
T_R reference temperature (K)
T_{ta} target temperature (K)
ν_A stoichiometric coefficient of reactant A
V_A volume of reactant A (m^3)
V_B volume of reactant B (m^3)

Greek Symbols

γ dimensionless activation energy
ε distribution coefficient
θ dimensionless time
ρ_l density of the liquid phase (mol m^{-3})
P_s density of the solid phase (mol m^{-3})
τ dimensionless temperature
τ_0 dimensionless initial temperature
τ_{cool} dimensionless cooling temperature
τ_{ta} dimensionless target temperature
τ_{max} dimensionless maximum temperature
$\Delta\tau_{ad,0}$ dimensionless adiabatic temperature rise
$\Delta\tau_{dis}$ dimensionless dissolution heat
μ_2' second moments of distribution
μ_3' third moments of distribution
ϑ polydispersity of the solid
δ mass transfer coefficients (cm s^{-1})
η_A dimensionless concentration of reactant A
η_B dimensionless concentration of reactant B
η_v dimensionless volume of solid reactant
η_d dimensionless diameter
α^* *Da* dimensionless cooling number

Abbreviations

SBR semibatch reactor
BR batch reactor
MAT maximum allowable temperature
QFS quick onset, fair conversion, smooth temperature profile
CA citric acid

REFERENCES

(1) Westerterp, K. R.; Molga, E. J. Safety and Runaway Prevention in Batch and Semibatch Reactors-A Review. *Chem. Eng. Res. Des.* **2006**, *84* (7), 543−552.
(2) Zhang, H.; Bai, M.; Wang, X.; Gai, J.; Shu, C.; Roy, N.; Liu, Y. Thermal runaway incidents-a serious cause of concern: An analysis of runaway incidents in China. *Process Saf. Environ. Prot.* **2021**, *155*, 277−286.
(3) Juncheng, J.; Dan, W.; Lei, N.; Gang, F.; Yong, P. Inherent thermal runaway hazard evaluation method of chemical process based on fire and explosion index. *J. Loss Prev. Process Ind.* **2020**, *64*, 104093.
(4) Semenoff, N. Zur Theorie des Verbrennungsprozesses. *Z. Phys. A: Hadrons Nucl.* **1928**, *48* (7), 571−582.
(5) Hugo, P.; Steinbach, J. A comparison of the limits of safe operation of a SBR and a CSTR. *Chem. Eng. Sci.* **1986**, *41* (4), 1081−1087.
(6) Steensma, M.; Westerterp, K. R. Thermally safe operation of a cooled semi-batch reactor - slow liquid-liquid reactions. *Chem. Eng. Sci.* **1988**, *43* (8), 2125−2132.
(7) Steensma, M.; Westerterp, K. R. Thermally safe operation of a semibatch reactor for liquid-liquid reactions-fast reactions. *Chem. Eng. Technol.* **1991**, *14* (6), 367−375.
(8) Steensma, M.; Westerterp, K. R. Thermally safe operation of a semibatch reactor for liquid-liquid reactions. Slow reactions. *Ind. Eng. Chem. Res.* **1990**, *29* (7), 1259−1270.
(9) Maestri, F.; Rota, R. Thermally safe operation of liquid−liquid semibatch reactors part II: single diffusion controlled reactions with arbitrary reaction order. *Chem. Eng. Sci.* **2005**, *60* (20), 5590−5602.
(10) Maestri, F.; Rota, R. Thermally safe operation of liquid−liquid semibatch reactors. part I: single kinetically controlled reactions with arbitrary reaction order. *Chem. Eng. Sci.* **2005**, *60* (12), 3309−3322.
(11) Maestri, F.; Rota, R. Temperature diagrams for preventing decomposition or side reactions in liquid-liquid semibatch reactors. *Chem. Eng. Sci.* **2006**, *61* (10), 3068−3078.
(12) Ni, L.; Mebarki, A.; Jiang, J.; Zhang, M.; Dou, Z. Semi-batch reactors: thermal runaway risk. *J. Loss Prev. Process Ind.* **2016**, *43*, 559−566.
(13) Guo, Z.; Feng, W.; Li, S.; Zhou, P.; Chen, L.; Chen, W. Facile approach to design thermally safe operating conditions for isoperibolic homogeneous semibatch reactors involving exothermic reactions. *Ind. Eng. Chem. Res.* **2018**, *57* (32), 10866−10875.
(14) Guo, Z.; Chen, L.; Chen, W. Development of extended boundary diagrams to design thermally safe operating conditions for homogenous semibatch reactors. *Chem. Eng. Sci.* **2018**, *189*, 24−32.
(15) Bai, W.; Hao, L.; Guo, Z.; Liu, Y.; Wang, R.; Wei, H. A new criterion to identify safe operating conditions for isoperibolic homogeneous semi-batch reactions. *Chem. Eng. J.* **2017**, *308*, 8−17.
(16) Han, Y.; Liu, Y.; Bai, W.; Ren, C.; Xu, L. Identification and prediction of inherently safe operating conditions for single diffusion controlled liquid-liquid heterogeneous reactions performed in isoperibolic semibatch reactors. *Chem. Eng. J.* **2021**, *421*, 129708.
(17) Zhang, B.; Hao, L.; Hou, H.; Zhu, J.; Dang, L.; Wei, H. A multi-feature recognition criterion for identification of thermally safe operating conditions for single kinetically-controlled reactions occurring in isoperibolic liquid-liquid semibatch reactors. *Chem. Eng. J.* **2020**, *382*, 122818.
(18) Jiang, J.; Jiang, J.; Wang, Z.; Pan, Y. Thermal runaway criterion for chemical reaction systems: a modified divergence method. *J. Loss Prev. Process Ind.* **2016**, *40*, 199−206.
(19) Kummer, A.; Varga, T.; Nagy, L. Semi-batch reactor control with NMPC avoiding thermal runaway. *Comput. Chem. Eng.* **2020**, *134*, 106694.
(20) Casson, M.; Lister, D. G.; Milazzo, M. F.; Maschio, G. Comparison of criteria for prediction of runaway reactions in the sulphuric acid catalyzed esterification of acetic anhydride and methanol. *J. Loss Prev. Process Ind.* **2012**, *25* (1), 209−217.
(21) Kummer, A.; Varga, T. What do we know already about reactor runaway? - A review. *Process Saf. Environ. Prot.* **2021**, *147*, 460−476.
(22) Samoilenko, N. G.; Korsunskii, B. L.; Bostandzhiyan, V. A.; Il'ichev, A. V.; Kustova, L. V. Thermal explosion in a batch reactor charged with a liquid-solid heterogeneous system. *Russ. J. Phys. Chem. B* **2016**, *10* (6), 973−977.
(23) Samoilenko, N. G.; Bostandzhiyan, V. A.; Kustova, L. V.; Korsunskii, B. L.; Il'ichev, A. V. Thermal explosion of a liquid-solid heterogeneous system in a semibatch reactor. *Russ. J. Phys. Chem. B* **2017**, *11* (3), 436−442.
(24) Samoilenko, N. G.; Kustova, L. V.; Korsunskii, B. L.; Il'ichev, A. V. On a nonstationary theory of thermal explosion in a semi-batch reactor. Homogeneous systems. *Russ. J. Phys. Chem. B* **2016**, *10* (5), 785−790.
(25) Westerterp, K. R.; Lewak, M.; Molga, E. J. Boundary diagrams safety criterion for liquid phase homogeneous semibatch reactors. *Ind. Eng. Chem. Res.* **2014**, *53* (14), 5778−5791.

https://doi.org/10.1021/acsomega.2c02139
ACS Omega 2022, 7, 21207−21219

(26) Maestri, F.; Rota, R. Kinetic-free safe optimization of a semibatch runaway reaction: nitration of 4-Chloro Benzotrifluoride. *Ind. Eng. Chem. Res.* **2016**, *55* (50), 12786−12794.
(27) Maestri, F.; Rota, R. Safe and productive operation of homogeneous semibatch reactors involving autocatalytic reactions with arbitrary reaction order. *Ind. Eng. Chem. Res.* **2007**, *46* (16), 5333−5339.
(28) Xiang, B.; Truong, N. T. V.; Feng, L.; Bai, T.; Qi, C.; Liu, Q. Study of the Role of Sodium Citrate in Bitumen Liberation. *Energy Fuels* **2019**, *33* (9), 8271−8278.

https://doi.org/10.1021/acsomega.2c02139
ACS Omega 2022, 7, 21207−21219